



**HAL**  
open science

## Methodologies and uncertainty estimates for T – T 90 measurements over the temperature range from 430 K to 1358 K under the auspices of the EMPIR InK2 project

Helen Mcevoy, Dave Lowe, Robin Underwood, Michael de Podesta, Graham Machin, Maria-Jose Martin, Jose Mantilla, Joaquin Campos Acosta, Mohamed Sadli, Frederic Bourson, et al.

### ► To cite this version:

Helen Mcevoy, Dave Lowe, Robin Underwood, Michael de Podesta, Graham Machin, et al.. Methodologies and uncertainty estimates for T – T 90 measurements over the temperature range from 430 K to 1358 K under the auspices of the EMPIR InK2 project. Measurement Science and Technology, 2021, 32 (3), 10.1088/1361-6501/abc50f . hal-03672302

**HAL Id: hal-03672302**

**<https://cnam.hal.science/hal-03672302>**

Submitted on 3 Jan 2023

**HAL** is a multi-disciplinary open access archive for the deposit and dissemination of scientific research documents, whether they are published or not. The documents may come from teaching and research institutions in France or abroad, or from public or private research centers.

L'archive ouverte pluridisciplinaire **HAL**, est destinée au dépôt et à la diffusion de documents scientifiques de niveau recherche, publiés ou non, émanant des établissements d'enseignement et de recherche français ou étrangers, des laboratoires publics ou privés.

Copyright

# Methodologies and uncertainty estimates for $T - T_{90}$ measurements over the temperature range from 430 K to 1358 K under the auspices of the EMPIR InK2 project

H C McEvoy<sup>1</sup>, D H Lowe<sup>1</sup>, R Underwood<sup>1</sup>, M de Podesta<sup>1</sup>, G Machin<sup>1</sup>, M J Martin<sup>2</sup>, J M Mantilla<sup>2</sup>, J Campos<sup>3</sup>, M Sadli<sup>4</sup>, F Bourson<sup>4</sup>, S Briau<sup>4</sup>, S G R Salem<sup>4,5</sup>, K Anhalt<sup>6</sup>, M Wachmer<sup>6</sup>, D R Taubert<sup>6</sup>, X J Feng<sup>7</sup>, J T Zhang<sup>7</sup>, X F Lu<sup>7</sup>, H Yoon<sup>8</sup>

<sup>1</sup> National Physical Laboratory, United Kingdom, <sup>2</sup>Centro Español de Metrología, Spain, <sup>3</sup>Agencia Estatal Consejo Superior de Investigaciones Científicas, Spain, <sup>4</sup>Laboratoire Commun de Métrologie LNE-Cnam, France, <sup>5</sup>National Institute for Standards, Tersa Street, Haram, Giza, 12211, Egypt, <sup>6</sup>Physikalisch-Technische Bundesanstalt, Germany, <sup>7</sup>National Institute of Metrology, China, <sup>8</sup>National Institute of Standards and Technology, USA

## 1 ABSTRACT

We report new developments in instrumentation and techniques for both acoustic (speed of sound) and radiometric primary thermometry methods. These include both new cylindrical resonators for extending acoustic gas thermometry to higher temperatures and absolute radiation thermometers incorporating InGaAs detectors to extend primary radiometry to lower temperatures than can be achieved using Si-detector based instruments. These new approaches have been established in order to determine the difference between thermodynamic temperature,  $T$ , and the International Temperature Scale of 1990 (the ITS-90),  $T_{90}$ , over the temperature range from 430 K to 1358 K as part of the three-year EMPIR project ‘Implementing the new kelvin 2’ (InK2). This paper describes the facilities and measurement methodologies for measuring  $T - T_{90}$  at each of the different institutes, along with an assessment of the target uncertainties. The work is ongoing, but we anticipate that the results of these measurements will ultimately be pooled to provide consensus values of  $T - T_{90}$  with associated estimated uncertainties. These consensus values will initially feed into the technical annex of the *mise en pratique* for the definition of the kelvin (MeP-K-19) and, if required, will be used to help to provide a foundation for any future temperature scale.

Key Words: temperature, thermodynamic temperature, ITS-90, blackbody, radiation thermometer, radiometer, thermodynamic, primary thermometry

## 2 INTRODUCTION

The current International Temperature Scale of 1990 (ITS-90) is the underpinning scale for temperature measurement worldwide. It defines instruments and methodologies (such as interpolation equations) for establishing a scale which is close to thermodynamic temperature, for temperatures above 0.65 K [1]. The instrumentation includes reference artefacts (fixed points which are based on phase transitions of pure materials) to calibrate specified thermometers: standard platinum resistance thermometers (SPRTs) for temperatures from  $\sim 14$  K up to 1235 K and infrared radiation thermometers above 1235 K. The temperatures assigned to the fixed points were based on measurements made using the best determinations of thermodynamic temperature prior to 1990. Subsequent measurements have highlighted small departures of the ITS-90 from thermodynamic temperature across the range from 20 K to 1235 K [2], with the uncertainty in the difference being especially large above about 693 K

(the Zn point) and corrections are needed to the ITS-90 values to obtain thermodynamic temperature.

The *European Metrology Programme for Innovation and Research* (EMPIR) project ‘Implementing the new kelvin 2’ (InK2) was established to investigate the differences between thermodynamic temperature,  $T$ , and the ITS-90 temperature,  $T_{90}$ , using different thermodynamic techniques. Its predecessor the *European Metrology Research Programme* (EMRP) project ‘Implementing the new kelvin 1’ (InK1) [3] determined thermodynamic temperatures for a selected set of metal carbon eutectic and the copper fixed points ( $\geq 1358$  K) [4] as well as a range of temperatures below the indium point (430 K). InK2 is concerned with completing the lower temperature evaluation of  $T - T_{90}$ , as well as determining  $T - T_{90}$  values from 430 K to 1358 K. The thermodynamic temperature data underpinning the specialist low temperature scale, the Provisional Low Temperature Scale of 2000 (PLTS-2000), was also a focus of study in the InK1 and InK2 projects.

This paper describes the methodology and progress towards achieving the target uncertainties for measurements of the differences  $T - T_{90}$  over the temperature range from 430 K up to 1358 K using two different thermodynamic techniques: acoustic thermometry and primary radiation thermometry (or radiometry). Measurements using these techniques are being carried out at: the National Physical Laboratory (NPL), UK; Centro Español de Metrología (CEM) in conjunction with the Agencia Estatal Consejo Superior de Investigaciones Científicas (IO-CSIC), Spain; the Conservatoire national des arts et métiers (Cnam) and the Laboratoire national de métrologie et d’essais (LNE), France; Physikalisch-Technische Bundesanstalt (PTB), Germany; and the National Institute of Metrology (NIM), China. The final results will be presented in a subsequent paper.

### 3 INSTRUMENTATION AND METHODOLOGY

The instrumentation and methodology being employed at each of the partner institutes, namely acoustic (NPL and NIM) and radiometric (NPL, CEM/ IO-CSIC, LNE-Cnam, PTB and NIM), are described in the following sections along with anticipated target uncertainties.

#### 3.1 ACOUSTIC GAS THERMOMETRY

##### 3.1.1 Introduction

Acoustic Gas Thermometry (AGT) [5] makes use of the simple relationship between thermodynamic temperature  $T$  and the limiting zero-pressure speed of sound,  $u_0$ , in a monatomic gas:  $u_0^2 = \gamma_0 kT/m$ , where  $k$  is the Boltzmann constant,  $m$  is the average molecular mass of the gas, and  $\gamma_0$  is the limiting low-pressure value of the adiabatic index, which is equal to exactly 5/3 in a monatomic gas.

In high accuracy AGT, the speed of sound  $u(T, p)$  is determined from the acoustic resonance frequencies of a gas-filled cavity. The shape of this cavity is either cylindrical, spherical or quasi-spherical. The resonance frequencies of a subset of acoustic modes are measured at several gas pressures and a single temperature (an isotherm), and a physical model describing the pressure dependence of  $u(T, p)$  is fitted to the data to find  $u_{0,T}$ .

### 3.1.2 Measurements at NPL

#### 3.1.2.1 Equipment and Methodology

In the previous InK project (InK1) NPL carried out extensive measurements of  $T - T_{90}$  over the temperature range from 118 K to 303 K using the NPL-Cranfield combined microwave and acoustic quasi-spherical copper resonator filled with argon. The measurements were made using relative AGT [5]. In relative AGT measurements are made of the ratios of  $u_0^2$  at the triple point of water,  $T_{TPW}$ , (273.16 K) to  $u_0^2$  at an unknown temperature  $T$ .  $T$  is then calculated from:

$$\frac{T}{273.16 \text{ K}} = \frac{m_T}{m_{TPW}} \left( \frac{u_{0,T}}{u_{0,TPW}} \right)^2 \quad (1)$$

where  $m_T$  and  $m_{TPW}$  are the average molecular masses of the gases used at  $T$  and  $T_{TPW}$ , respectively. The mass terms will cancel if the same gas is used for both temperatures, and if the composition of this gas remains stable with temperature and time.

The  $T - T_{90}$  values obtained with this method and apparatus agreed with previous estimates of  $T - T_{90}$  but had significantly lower uncertainties. In addition, previously undetected detail was observed in the  $T - T_{90}$  curve due to the use of small temperature intervals between measurements [6, 7].

The NPL AGT work in the InK2 project builds on the capability developed in the previous project and extends the measurement range to higher temperatures. In order to do this, it has been necessary to rethink every aspect of the system design, but the most fundamental change has been in moving from a quasispherical resonator to a cylindrical resonator [8]. This change is favoured because of the combination of several effects.

The acoustic transducers typically used in acoustic resonators have a maximum operating temperature of 423 K, and so at high temperatures they can no longer be placed directly on the resonator surface. One option for overcoming this limitation is to couple sound into and out of the resonator using acoustic waveguides. In order to minimally perturb the resonances, the acoustic waveguides must be relatively small in diameter, and hence will have limited high-frequency transmission. However, as the speed of sound increases with temperature ( $u \propto \sqrt{T}$ ), the frequency of acoustic resonances in a resonator of a fixed size also increases. Thus, to have as many resonances to measure as possible, it is necessary to increase the size of the resonator.

Making increasingly larger spheres is one option, but the overall system volume and mass scale as the resonator radius squared and cubed respectively. When coupled with issues of material creep and operation at high temperatures and pressures, there comes a point where switching to a long cylindrical resonator becomes advantageous. This is because, in a long cylinder, the extra axial length results in a number of non-degenerate modes with relatively low frequencies (Figure 1). Additionally, manufacturing is simpler and all entry and exit ports (for acoustics, microwaves, and gas) can be positioned on a single endplate, simplifying access (Figure 2). One final advantage of the cylindrical geometry is the length-to-radius ratio can be chosen to minimise the number of accidental degeneracies. The reason for wanting to measure as many modes as possible is that the key uncertainties are likely to arise from inadequate understanding of the physical processes occurring within the resonator. Whereas measurements of even a single acoustic mode would be sufficient to estimate the temperature *in principle*, the extent of

agreement between multiple acoustic modes with different characteristics provides a strong test of the completeness of the theoretical understanding of the physics underlying the temperature estimates.

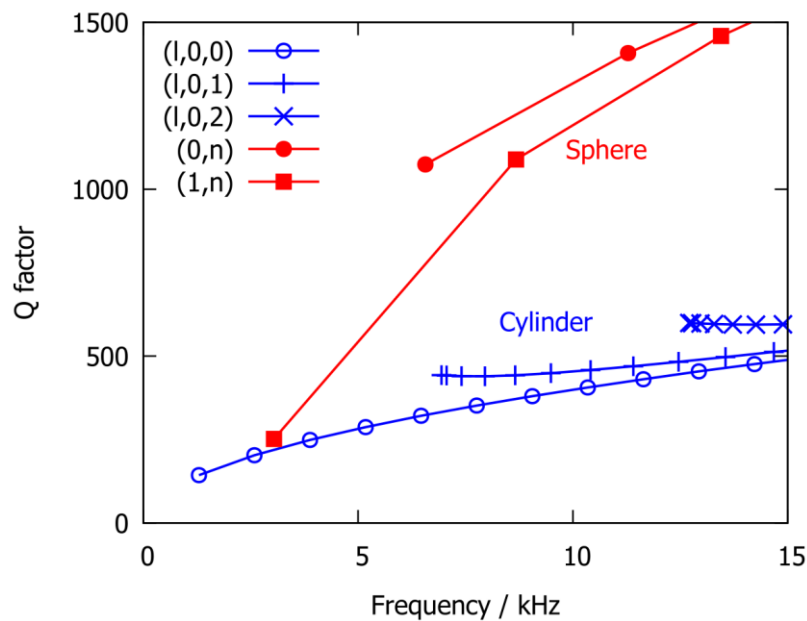


**Figure 1:** Graph showing the quality factor of acoustic modes available for measurement in cylinders (blue) and spheres (red) as a function of frequency. The calculation is made for a cylinder of radius 50 mm and length 220 mm and a sphere of radius 62 mm at the melting temperature of aluminium ( $T = 933 \text{ K}$ ) in one atmosphere ( $p = 100 \text{ kPa}$ ) of argon. Notice that for frequencies below 15 kHz, many more modes are available for study in the cylinder compared with the sphere, however their quality factor is substantially lower.

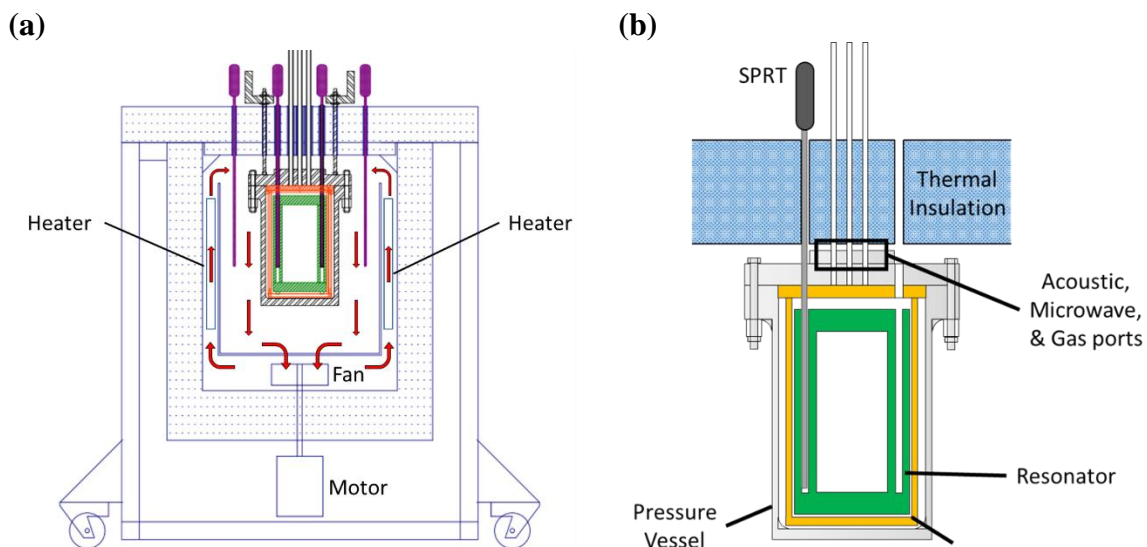


**Figure 2:** Schematic design of the NPL INK2 cylindrical resonator (a) Overview (b) Resonator Detail

As with quasispherical resonators, simultaneous microwave measurements facilitate compensation of the acoustic measurements for temperature- and pressure-induced

dimensional changes. At higher temperatures, dimensional changes in the cylindrical resonator from material creep are also likely to be significant.

In cylinders, mode-degeneracy is also a complicating factor for certain electromagnetic mode classes. For example, the  $TE0pq$  modes (which have the advantages of high quality-factors and zero current density at the lid-cylinder interface [8]) are frequency-degenerate with the low quality-factor  $TM1pq$  modes. This degeneracy can be lifted by making the cylinder cross-section slightly non-circular (Figure 3). Alternatively, if a multi-port vector network analyser is available, two antennas may be used to detect resonances in different locations in the cylinder. Because of the orthogonal nature of the electromagnetic field patterns on resonance, the two signals may then be combined to isolate each of the degenerate resonances in turn.

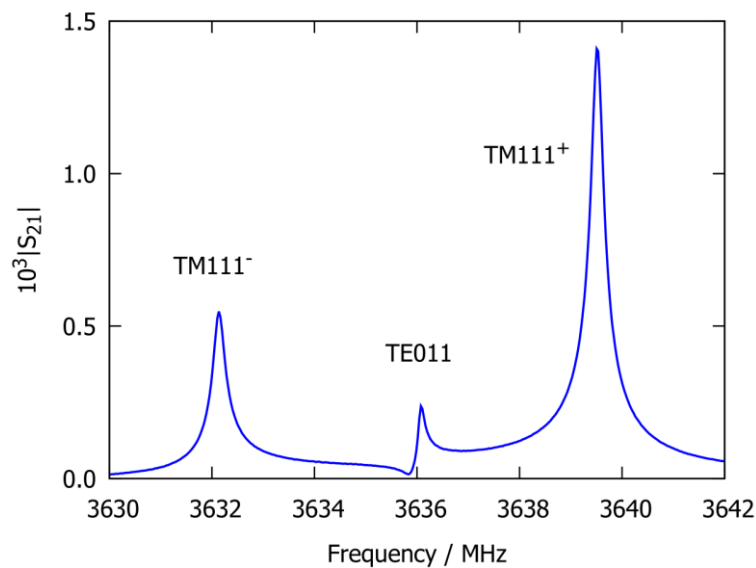


**Figure 3: The lifting of degeneracy of microwave modes in a cylinder with an ellipsoidal cross section. The  $TM111$  doublets are raised and lowered in frequency, allowing access to the unperturbed  $TE011$ .**

### 3.1.2.2 Early results and target uncertainties

Figure 4 shows the spontaneous fractional changes in length and radius observed in an aluminium resonator held at 429 K (the In point). This so-called ‘creep’ arises from growth of precipitated impurities introduced to harden the alloy for use at lower temperatures. Although the resonator changed size significantly during the measurement period, the rate of change was slow enough to allow acoustic resonance data to be compensated, thus allowing the speed of sound to be estimated.

Figure 5 shows mode-by-mode estimates of thermodynamic temperature derived from acoustic measurements at 323 K and 429 K using *absolute* primary acoustic gas thermometry i.e. the results are based directly on  $u_0^2 = \gamma_0 kT/m$  rather than ratio of speed of sound measurements described in Equation 1. The results are shown as differences from the expected results based on estimates of the difference between  $T$  and the ITS-90 published by BIPM CCT in 2011 [2]. The magnitude of the differences is typically  $\pm 20$  parts in  $10^6$  in the speed of sound which amounts to approximately 13 mK at 323 K and 17 mK at 429 K. Agreement at this level is indicative of being able to fully model the physics within the resonator. Notice that since the deviations are systematic, simply taking an average over all the modes will not guarantee convergence to the correct answer.

Most significant is the similarity of the deviations from one temperature to another. Because of this we expect that *relative* primary acoustic gas thermometry (Equation 1), in which mode-by-mode ratios of changes in the speed-of-sound squared are taken, will produce thermodynamic temperature estimates with uncertainties of just a few millikelvin.

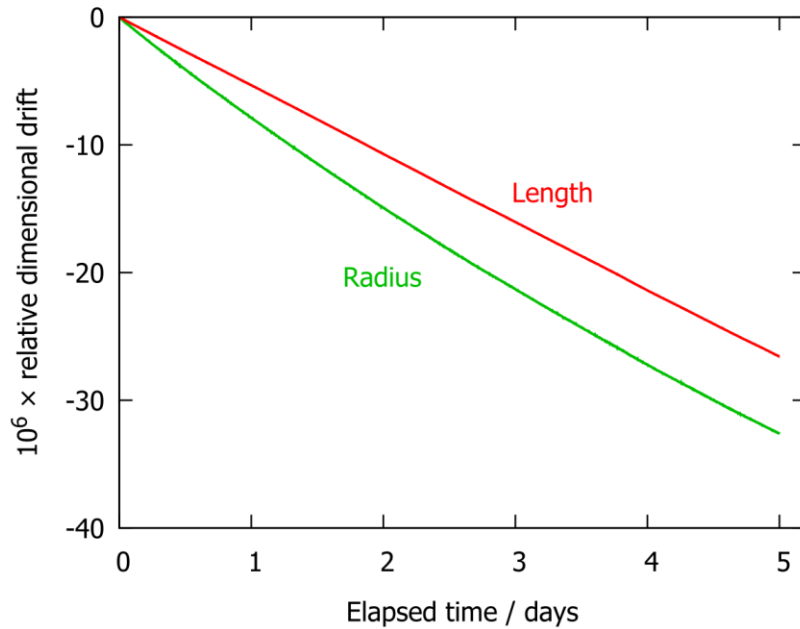
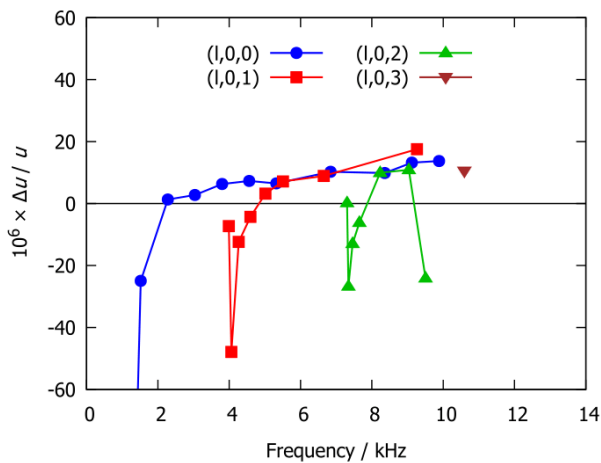


Figure 4: Dimensional creep in an aluminium cylinder held at 429 K. The changes in length and radius are very significant, but slow enough that that microwave measurements can be used to compensate.

(a) 323 K



(b) 429 K

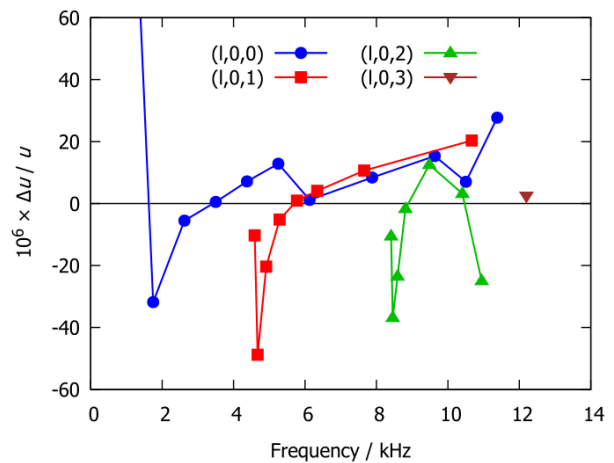


Figure 5: The results of absolute primary acoustic gas thermometry at (a) 323 K and (b) 429 K. The results are shown as deviations in the speed of sound in argon from the expected results based on estimates of the difference between  $T$  and ITS-90 published by BIPM CCT in 2011 [2]. 20 parts in  $10^6$  corresponds to approximately 13 mK at 323 K and 17 mK at 429 K

### 3.1.2.3 Next steps

Going forward, NPL will use a cylindrical resonator constructed out of a copper alloy - CuCrZr. This alloy is known to retain its hardness up to 873 K while still retaining 80 % - 90% of the thermal and electrical conductivity of copper. This new resonator will be used to perform

$T - T_{90}$  measurements up to higher temperatures than can be reached using the aluminium resonator.

### 3.1.3 Measurements at NIM

Since 2013 NIM has been working to develop acoustic gas thermometry for use up to the copper point (1358 K) using cylindrical resonators [9, 10, 11]. The design of the acoustic transducers was optimised to obtain a good signal-to-noise ratio at high temperature [12]. Because acoustic waveguides with larger inner diameter (ID) and shorter length have smaller acoustic attenuation but larger perturbation to the acoustic resonant frequencies, it is necessary to design the waveguides to get a good balance between the sound attenuation and perturbation. The basic idea of the waveguide design is to use a smaller ID duct near the resonator cavity and then use a larger ID duct for most of the sound transfer. We have calculated the effects for different sizes of acoustic waveguides based on the impedance theory [13]. By using the variable inner diameter acoustic waveguides, the perturbation due to the resonant frequency from the acoustic waveguides can be controlled to less than  $1 \times 10^{-5}$ , and the random error for the acoustic resonant frequencies, which refers to the typical fitting uncertainty of one resonance, can be reduced to less than  $2 \times 10^{-6}$  at 900 K for the acoustic resonant measurements with a welded cylindrical cavity. The largest uncertainty component for the thermal expansion determination is from the inconsistency between different microwave modes, which is about  $1.3 \times 10^{-5}$  near 900 K [10].

Heat pipes are used to provide a uniform and stable temperature environment for the cylindrical cavity [14]. At temperatures from 323 K to the 505 K, a homemade water heat pipe is used. By the additional controlling of the temperature of the pressure vessel, the temperature stability of the cylindrical resonator is within  $\pm 1$  mK over 30 minutes, and the uniformity of the resonator is 2 mK near 505 K.

Continuous improvements and measurements with high temperature acoustic gas thermometry at NIM are ongoing with the objective of achieving uncertainties for the  $(T - T_{90})$  measurement near 500 K, 1000 K and 1358 K of 10 mK, 50 mK and 120 mK, respectively, with  $k = 2$ .

## 3.2 PRIMARY RADIATION THERMOMETRY AND RADIOMETRY

### 3.2.1 Introduction

Primary radiometry techniques determine thermodynamic temperatures by measuring the absolute spectral radiance ( $\text{W m}^{-2} \text{sr}^{-1} \text{nm}^{-1}$ ) of a blackbody source [15, 16]. The method requires the determination of the radiance (radiant flux emitted per unit area and unit solid angle) in a finite wavelength band (nm) with optical power measurements traceable to a cryogenic electrical substitution radiometer. Several different methods based on this principle exist [17], differing in where the defining geometry (two parallel, circular, collinear apertures of known physical dimensions and separation) is located in the calibration chain and whether an imaging system is used.

For InK2 a number of different primary radiation thermometers and radiometer systems, operating at different wavelengths, are being used to determine  $T$ , either directly or indirectly, and hence infer  $T - T_{90}$ . Measurements are being made of:

- fixed-point blackbody (FPB) sources of tin (505 K), zinc (693 K), aluminium (933 K), silver (1235 K), gold (1337 K) and copper (1358 K)
- variable temperature heat pipe blackbody (VTBB) sources which incorporate contact thermometers which have been calibrated according to the ITS-90.

The instrumentation, calibration process and measurement regime used by each of the participants (NPL, LNE-Cnam, CEM/ IO-CSIC, PTB and NIM) will now be described.

### 3.2.2 Measurements at NPL

#### 3.2.2.1 Equipment and methodology

The primary radiation thermometer used for the NPL measurements is the Near Infrared Radiation Thermometer 3 (NIRT3) developed by the National Institute of Standards and Technology (NIST), USA [18]. It is an InGaAs detector-based radiation thermometer operating at a wavelength of  $\sim 1600$  nm, with good optical and linearity characteristics. It is shown schematically in Figure 6.

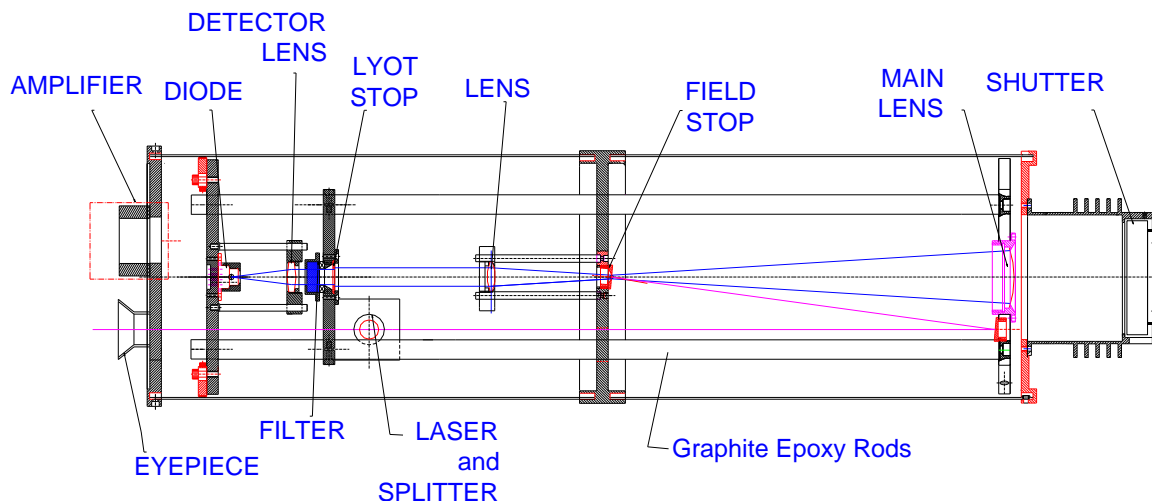


**Figure 6: Schematic of the NIST NIRT3 (courtesy of NIST)**

In order to determine  $T$  from the thermometer output the instrument needs to be calibrated in terms of absolute spectral responsivity. The spectral responsivity of the NIRT3 was measured at NIST using the NIST spectral irradiance responsivity and spectral radiance responsivity (SIRCUS) facility [19] traceable to the NIST Primary Optical Watt Radiometer. However, due to some technical difficulties (and therefore larger uncertainties) associated with absolutely calibrating an InGaAs-type detector (rather than a silicon photodiode detector) using this facility, it was decided instead to anchor the absolute calibration of the NIRT3 using, as a reference, the NIST gold FPB. The thermodynamic temperature of the NIST gold point was determined using the NIST 650 nm Absolute Pyrometric Transfer Radiometer (APXR650), which had been calibrated using SIRCUS. The thermodynamic temperature of the NIST gold point was determined to be 1337.36 K using the APXR650 (i.e. 30 mK above the current ITS-90 value) with an estimated uncertainty of 81 mK ( $k = 2$ ).

To determine thermodynamic temperatures with the NIRT3 the expected signals at each required temperature are calculated from the spectral responsivity (from the NIRT3 SIRCUS calibration) and Planck's law. The expected signals are then adjusted using the results of the measurements at the gold fixed point (with assigned  $T = 1337.36$  K). The adjusted expected signals are then compared to the actual signals obtained at each temperature to determine  $T - T_{90}$ . For measurements with the NIRT3 at NPL the reference is the NPL gold FPB (estimated emissivity 0.99998). This is assumed to have the same thermodynamic temperature as the NIST gold point within the measurement uncertainties.

At NPL  $T - T_{90}$  values are being determined using both FPBs and heat pipe VTBBs. The former are high emissivity (at least 0.99997) graphite blackbody cells, containing high purity metals of, respectively, tin, zinc, aluminium, silver and copper. The copper cell [20] is installed in an electrical furnace with three heated zones. The other cells are installed within a heat pipe liner within a furnace: a potassium heat pipe in a furnace with three heated zones for the tin and zinc cells and a sodium heat pipe in a single-heated-zone furnace for the aluminium and silver cells. The heat pipes improve the temperature uniformity of the heated zone in which the cell sits, and hence improve the fixed-point freezing plateau duration and shape. (Note that the tin point temperature is below the minimum operating temperature of the potassium heat pipe, but using a furnace with three heated zones enables the required level of temperature uniformity to be achieved at the tin point temperature.)

One of the NPL VTBBs is a bespoke pressure-controlled heat pipe (PCHP) system from Advanced Cooling Technologies (ACT), USA to NPL's design and technical specification. The facility consists of two heatpipes: a potassium PCHP for the 673 K to 1173 K temperature range and a sodium PCHP for 973 K to 1373 K range, with a single control unit. The potassium heat pipe is constructed from Inconel whereas the sodium heat pipe is constructed from Haynes alloy - a nickel-chromium tungsten-molybdenum alloy material - which gives it more structural strength and enables it to reach the Cu fixed-point temperature (1358 K). Each PCHP incorporates a high emissivity ( $\sim 0.99996$ ) blackbody cavity nominally 400 mm long, 12.5 mm diameter with a 120° end cone. Each PCHP also contains five thermometer wells to insert calibrated thermometers (standard platinum resistance thermometers and Au/Pt thermocouples). The contact thermometers have been calibrated in terms of ITS-90 using fixed-point cells. A schematic of the system is shown in Figure 7.

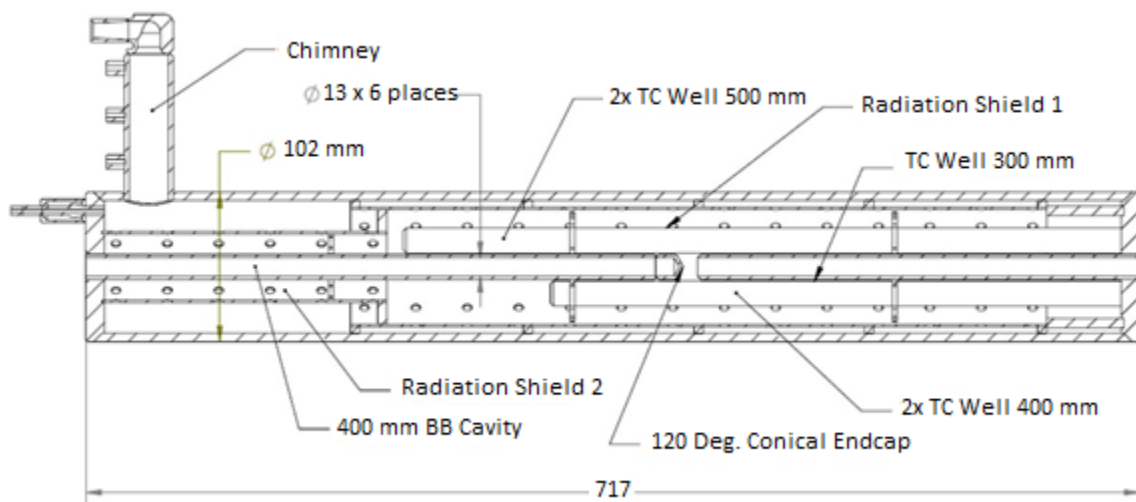


Figure 7: Schematic of one of the PCHPs (courtesy of Advanced Cooling Technologies Inc)

Additionally, measurements are being performed using a ‘passive’ caesium heat pipe source which can cover the temperature range from 573 K to 873 K. This incorporates a blackbody cavity of nominally 15 mm diameter and 200 mm length, and which has an estimated emissivity of 0.9997. Four thermometer wells run from the rear of the heat pipe partially along the length of the blackbody cavity.

In every case  $T - T_{90}$  is determined by comparing the thermodynamic temperature as measured by the NIRT3 with the corresponding ITS-90 temperature, either ITS-90 temperature of the fixed-point metal or the temperature given by the calibrated contact sensors in the rear of the PCHP.

### 3.2.2.2 Target uncertainties

Example target uncertainties for the measurements of the FPBs and VTBBs at NPL are given in Tables 1 to 3 below. The uncertainties are comprised of both the uncertainty associated with the calibration of the NIRT3 and the uncertainty associated with the FPB or VTBB. The former includes components for the measurement of the spectral responsivity of the NIRT3, the measurement of the gain ratios and the uncertainty in the assignment of  $T$  to the NIST Au point since this was used to initially calibrate the NIRT3.

The uncertainties associated with the FPB and VTBB are estimated using the Consultative Committee of Thermometry non-contact thermometry working group (CCT-WG5) document ‘Uncertainty Budgets for Calibration of Radiation Thermometers below the Silver Point’ [21] and also include the uncertainty associated with the NPL Au point ( $U = 22$  mK ( $k = 2$ )), since this is used as the reference to calibrate the NIRT3 in use.

**Table 1: Example target uncertainties associated with the NIRT3 at the fixed-point temperatures of Zn (693 K) and Ag (1235 K) with reference to the NPL Au point**

Source of Uncertainty	At Zn point $u/$ mK	At Ag point $u/$ mK
NIRT spectral responsivity calibration	16	50
Amplifier gain drift/calibration	2	0
Au point uncertainty	3	10
Voltmeter accuracy	1	1
NIRT3 SSE/ thermal profile	1	1
<b>Total uncertainty (<math>k = 1</math>)/ mK</b>	<b>16</b>	<b>51</b>
<b>Total expanded uncertainty (<math>k = 2</math>)/ mK</b>	<b>33</b>	<b>102</b>

**Table 2: Example target uncertainties for the measurements of the FPBs using the NIRT3**

Source of uncertainty	At Zn point $u/$ mK	At Ag point $u/$ mK
Impurities	0.3	0.7
Plateau Identification	2.0	2.0
Isothermal blackbody emissivity	0.4	2.9
Emissivity calculation	0.9	1.2
Reflected ambient radiation	0.0	0.0
Radiant heat exchange	0.3	3.2
NIRT3 component	16.0	51.0
<b>Total uncertainty (<math>k = 1</math>)/ mK</b>	<b>16</b>	<b>51</b>
<b>Total expanded uncertainty (<math>k = 2</math>)/ mK</b>	<b>32</b>	<b>102</b>

**Table 3: Example target uncertainties for the measurements of the PCHPs with the NIRT3**

Source of uncertainty	Using the K PCHP at the Zn point, $u (k = 1)/ \text{mK}$	Using the Na PCHP at the Ag point, $u (k = 1)/ \text{mK}$
Isothermal blackbody emissivity	1.0	4.0
Emissivity calculation	3.1	9.8
Reflected ambient radiation	0.0	0.0
Radiant heat exchange	0.9	5.0
Convection	1.7	3.5
Cavity bottom uniformity	15.0	30.0
Ambient conditions	5.0	12.0
SPRT/ TC calibration	5.0	41.0
SPRT/ TC stability & TC ice point	3.0	8.0
Resistance Bridge accuracy	6.0	-
Resistance bridge resolution	0.6	-
Voltmeter calibration	-	20.0
Voltmeter drift	-	54.0
Voltmeter resolution	-	5.0
Radiometer component	16.0	51.0
<b>Total uncertainty (<math>k = 1</math>)/ mK</b>	<b>24</b>	<b>94</b>
<b>Total expanded uncertainty (<math>k = 2</math>)/ mK</b>	<b>49</b>	<b>188</b>

### 3.2.3 Measurements at CEM

#### 3.2.3.1 Equipment and methodology

$T - T_{90}$  measurements are being performed at CEM using two absolutely calibrated standard radiation thermometers (RTs) to measure both FPBs (Cu, Ag and Zn) and VTBBs. The standard thermometers are a silicon-detector-based LP4 (650 nm and 900 nm filters) and an InGaAs-detector based LP5 (1550 nm filter) [22, 23]. Both are calibrated by comparison with a Si trap radiometer and an InGaAs radiometer, respectively, using the radiance mode [17, 24]. The Si trap radiometer and the InGaAs radiometer are calibrated absolutely at IO-CSIC with an electrical substitution cryogenic radiometer.

The LP4 at 900 nm and LP5 at 1550 nm can also be used to estimate  $T$  by extrapolation (relative primary radiation thermometry) to lower temperatures from a Ag fixed point whose thermodynamic temperature,  $T_{\text{AgFP}}$ , has been assigned a value of 1234.90 K ( $U = 170 \text{ mK}$  ( $k = 2$ )) using the absolutely calibrated thermometer at 650 nm. The Ag cell is from ISOTECH and it is installed in a Na heat pipe ISOTECH OBERON R 426 furnace.

The method used to measure  $T$  (either absolute primary radiation thermometry or relative primary radiation thermometry) follows the scheme in Table 4. The indicated temperature ranges correspond to the range at which the radiation thermometers are most linear.

**Table 4: Different ways of measuring  $T$  at CEM**

Standard RT	Wavelength/ nm	Temperature range/ K	Absolute primary radiation thermometry	Relative primary radiation thermometry
LP4	650	> 1223	x	
LP4	900	> 1073	x	x
LP5	1550	673 – 1235	x	x

The VTBBs used for measuring  $T - T_{90}$  are a Na heat pipe and a Cs heat pipe from KE Technologie (see Figure 8). The temperatures of the two VTBBs are measured using two ISOTECH standard platinum resistance thermometers (SPRTs) one of  $25 \Omega$  for  $T_{90} \leq 873$  K and another of  $0.25 \Omega$  for  $T_{90} \geq 873$  K. The SPRTs have been calibrated at fixed points with an uncertainty of 10 mK and 20 mK, respectively. The SPRTs are placed in a thermowell within the heat pipe. For temperatures  $> 873$  K, the SPRT is protected with a platinum sheath and air circulation (ISOTECH 416 system) is used to prevent contamination.

A number of corrections are applied to the measurement results: the SPRT reading is corrected for conduction within the Inconel tube; the radiation thermometer reading is corrected for the dark current, the size-of-source effect (to take into account the difference between the effective radii of the Ag FP and VTBB, which was assessed by measuring the temperature profiles of the sources [25]) and the emissivity of the VTBB.

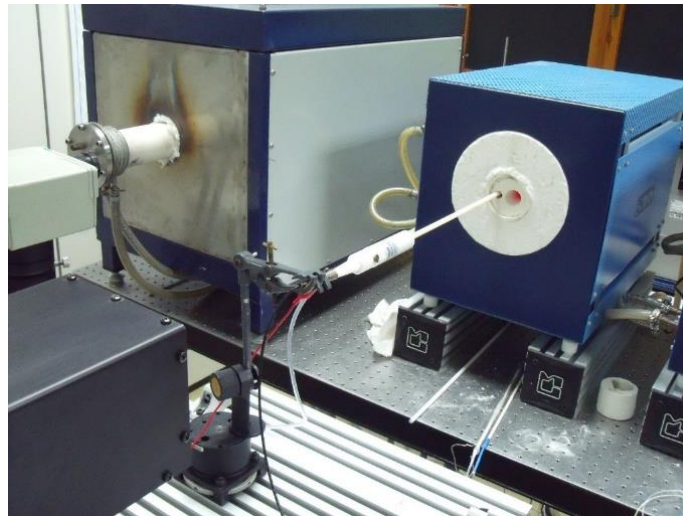


**Figure 8: Measurements of  $t-t_{90}$  in heat pipes using a SPRT and a radiation thermometer (RT). (Note: the field-of-view of the RTs is not blocked by the head of the SPRT)**

### 3.2.3.2 Uncertainties

#### 3.2.3.2.1 Uncertainties of the absolute calibration of the radiation thermometers

The estimation of uncertainties has been carried out using the method described in Appendix B of [26] and [27]. The uncertainty calculation is based on the key spectral parameters of the thermometers and follows the approach described in [27].

Table 5 shows the uncertainty budget for the temperature measurements using the LP4 at 650 nm. The components include the uncertainties associated with: the monochromator calibration and its drift; the standard deviation of the measurements of the spectral response; the uncertainty associated with  $H$  (the absolute calibration of the standard radiometer, its linearity and drift and the components related to the calibration by comparison), and the uncertainty associated with the radiation thermometer when in use (size-of-source effect, linearity and drift).

**Table 5: Uncertainty budget for absolute measurements with the LP4 at 650 nm, at  $T(\text{Cu})$ ,  $T(\text{Ag})$  and 1223 K showing  $u$  (total standard uncertainty,  $k = 1$ ) and  $U$  (total expanded uncertainty,  $k = 2$ )**

Uncertainty component	Value	Unit	Standard uncertainty	Contribution to the uncertainty/ mK		
				1357.77 K	1234.93 K	1223.15 K
$\lambda_0$ , monochr. calib.	0.03	nm	0.0300	43	41	41
$\lambda_0$ , drift	0.05	nm	0.0289	42	40	39
$\sigma$ , bandwidth	0.07	nm	0.0700	14	16	16
$H$ , trap detector (TD) calib.	0.075	%	0.0375	31	26	25
$H$ , aperture area	0.1	%	0.0500	42	35	34
$H$ , distance	0.02	%	0.0100	8	7	7
$H$ , spatial homog. source	0.12	%	0.0346	29	24	23
$H$ , source stability	0.01	%	0.0100	8	7	7
$H$ , diffraction	0.01	%	0.0100	8	7	7
$H$ , stray light	0.01	%	0.0029	2	2	2
$H$ , out of band	0.01	%	0.0029	2	2	2
$H$ , signal/noise	0.01	%	0.0029	2	2	2
$H$ , TD drift	0.05	%	0.0300	24	20	20
$H$ , TD linearity	0.1	%	0.0289	24	20	20
In use $S$ , SSE	0.004	%	0.0012	1	1	1
In use $S$ , linearity	0.06	%	0.0173	14	12	12
In use $S$ , drift	0.03	K	0.0087	9	9	9
<b>Total uncertainty (<math>k = 1</math>)/ mK</b>				<b>95</b>	<b>84</b>	<b>83</b>
<b>Total expanded uncertainty (<math>k = 2</math>)/ mK</b>				<b>190</b>	<b>170</b>	<b>170</b>

The sources of uncertainty for the absolute calibration of the LP4 at 900 nm and the LP5 at 1550 nm are determined in a similar way with appropriate values for the components included in the budget. The expanded uncertainties for the LP4 at 900 nm are 260 mK, 220 mK and 170 mK at 1358 K, 1235 K and 1073 K, respectively. Those for the LP5 at 1550 nm are 110 mK, 140 mK, 180 mK and 220 mK at 673 K, 773 K, 873 K and 973 K, respectively. The drift of the LP5 is considered negligible because it is measured every day at the reference Ag FP.

The uncertainties associated with the radiation thermometers (RTs) are combined with the uncertainties associated with the  $T_{90}$  measurements (SPRT calibration, uncertainty due to the conduction at the Inconel block, conduction and rotation of the SPRT in the VTBB insert, the resistance bridge and standard resistor, self-heating of the SPRTs, stability of the VTBB and drift of the SPRT) to give the overall uncertainties shown in Table 6.

**Table 6: Uncertainty budget for  $T - T_{90}$  measurements (absolute primary radiation thermometry)**

Uncertainty component	$T/ \text{K}$	$U/ \text{mK}$	$u/ \text{mK}$	Total combined uncertainties		
				$T/ \text{K}$	$u (T-T_{90})/ \text{K}$	$U (T-T_{90})/ \text{K}$
$T_{90}$ , SPRT and VTBB	673	39	19.5	673	<b>58</b>	<b>120</b>
	773	39	19.5	773	<b>73</b>	<b>150</b>
	873	39	19.5	873	<b>92</b>	<b>180</b>
	973	41	20.5	973	<b>112</b>	<b>220</b>
	1073	41	20.5	1073	<b>87</b>	<b>170</b>
	1223	41	20.5	1223	<b>87</b>	<b>170</b>
	Ag	-	-	Ag	<b>85</b>	<b>170</b>
	Cu	-	-	Cu	<b>95</b>	<b>190</b>
$T$ , RT	673	110	55			
	773	140	70			
	873	180	90			
	973	220	110			
	1073	170	85			
	1223	170	85			
	Ag	170	85			
	Cu	190	95			

3.2.3.2.2 Uncertainties of the  $T - T_{90}$  measurements using relative primary radiation thermometry

For the relative primary radiation thermometry measurements, the LP4 at 900 nm is measured at the CEM Ag fixed point, with assigned  $T = 1234.90 \text{ K}$ , as described above. Using the relative spectral responsivity of the LP4  $T$  is then calculated in a relative way. The uncertainty calculation is again based on [27] and includes the uncertainty in the LP4 calibration (monochromator calibration and drift, standard deviation of the measurements of the relative spectral response, uncertainty in assigning  $T_{\text{ref}}$  etc.) along with the uncertainty associated with the use of the thermometer (size-of-source effect, non-linearity and drift). Table 7 shows the overall uncertainty budget.

**Table 7: Uncertainty budget for the  $T$  measurements with the LP4 at 900 nm, at 1223 K and 1073 K.**

Uncertainty component	Value	Unit	$u$	Contribution to the uncertainty/ mK	
				At 1223 K	At 1073 K
$\lambda_0$ , monochr.	0.03	nm	0.0300	0.4	4.7
$\lambda_0$ , drift	0.05	nm	0.0289	0.4	4.5
$\sigma$ , bandwidth	0.05	nm	0.0500	0	0.7
$T_{\text{ref}}$	170	mK	85	83.4	64.2
$S_{\text{ref}}$	$4.00 \times 10^{-14}$	A	$4.00 \times 10^{-14}$	0.1	0.1
In use $S$ , SSE	0.006	%	0.0017	1.6	1.2
In use $S$ , linearity	0.062	%	0.0179	16.7	12.9
In use $S$ , drift	30	mK	9	8.7	8.7
<b>Total uncertainty (<math>k = 1</math>)/ K</b>				<b>86</b>	<b>66</b>
<b>Total expanded uncertainty (<math>k = 2</math>)/ K</b>				<b>170</b>	<b>130</b>

For the LP5 at 1550 nm the calculation is as above using appropriate values for the uncertainty components. The overall expanded uncertainties are 90 mK, 70 mK, 90 mK and 110 mK at 673 K, 773 K, 873 K and 973 K, respectively.

Table 8 shows the total measurement uncertainty including components associated with the SPRT and VTBB, and Table 9 summarises all the values from both radiometric methods highlighting the best values (indicated by an asterisk) when both methods are available.

**Table 8: Uncertainty budget of  $T - T_{90}$  measurements (relative primary thermometry)**

Uncertainty component	$T/ \text{K}$	$U/ \text{mK}$	$u/ \text{mK}$	Total combined uncertainties		
				$T/ \text{K}$	$u(T-T_{90})/ \text{mK}$	$U(T-T_{90})/ \text{mK}$
$T_{90}$ , SPRT and VTBB	673	39	19.5	673	<b>49</b>	<b>100</b>
	773	39	19.5	773	<b>40</b>	<b>80</b>
	873	39	19.5	873	<b>49</b>	<b>100</b>
	973	41	20.5	973	<b>59</b>	<b>120</b>
	1073	41	20.5	1073	<b>68</b>	<b>140</b>
	1223	41	20.5	1223	<b>87</b>	<b>170</b>
$T$ , RT	673	90	45			
	773	70	35			
	873	90	45			
	973	110	55			
	1073	130	65			
	1223	170	85			

**Table 9: Summary of  $T - T_{90}$  measurement uncertainties at CEM for different thermometers and primary radiation thermometry methods.**

Temperature/ K	Radiation thermometer	$U(T-T_{90})/ \text{mK} (k = 2)$	
		Absolute primary thermometry	Relative primary thermometry
1357.77	LP4, 650 nm	<b>190</b>	-
1234.93	LP4, 650 nm	<b>170</b>	-
1234.93	LP4, 900 nm	<b>220</b>	-
1223	LP4, 900 nm	<b>220</b>	<b>170*</b>
1073	LP4, 900 nm	<b>170</b>	<b>140*</b>
973	LP5, 1550 nm	<b>220</b>	<b>120*</b>
873	LP5, 1550 nm	<b>180</b>	<b>100*</b>
773	LP5, 1550 nm	<b>140</b>	<b>80*</b>
673	LP5, 1550 nm	<b>110</b>	<b>100*</b>

### 3.2.4 Measurements at LNE-Cnam

#### 3.2.4.1 Equipment and methodology

LNE-Cnam is using a radiance method to measure the thermodynamic temperature,  $T$ , of the Zn, Al and Ag fixed points, as well as a heatpipe VTBB. The measurements are carried out by comparing the radiance of the fixed points to that of a monochromatic source, which is absolutely calibrated against the LNE-Cnam cryogenic radiometer. The comparison is performed using LNE-Cnam's monochromator-based radiance comparator. This is generally used in the visible range but, for this work, it has been adapted to work in the infrared spectral range (around 1500 nm) using a suitable grating and an InGaAs photodiode detector.

Figure 9 shows an overview of the radiance comparator which, for the fixed point/monochromatic radiance source comparison, is translated in front of the bench containing the sources. The instrument is comprised of four main parts: A, B, C and D defining respectively the geometrical extent, the spectral range, the shape of the beam and the detection system.

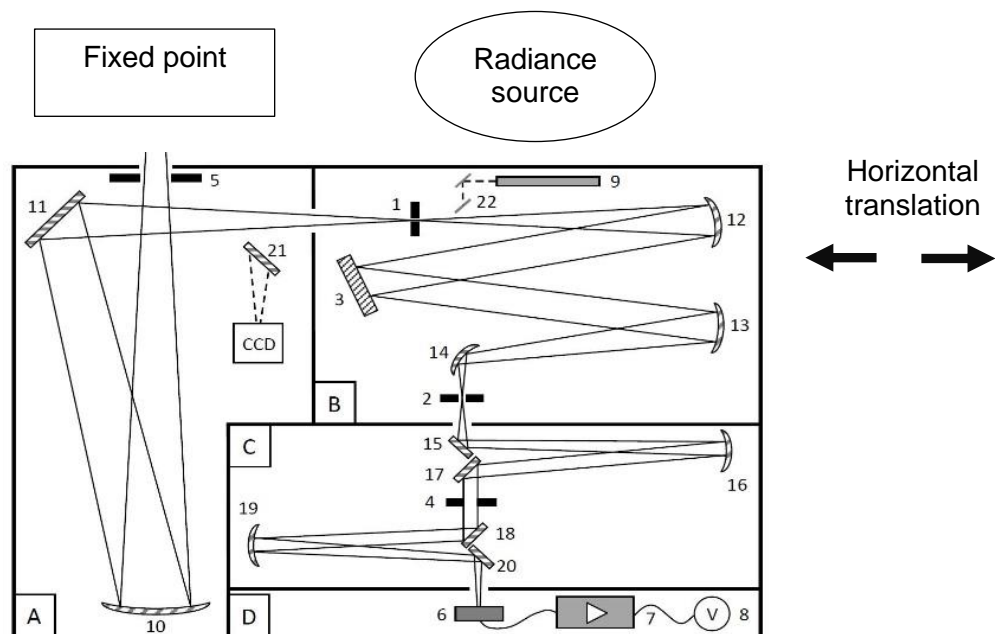


**Figure 9: Schematic view of the radiance comparator in front of the sources showing the: field stop and entrance slit of the monochromator (1), exit slit (2), grating (3), Lyot pupil (4), entrance pupil (5), signal output (6, 7 and 8), gold coated mirrors (10 to 20)**

The monochromatic source consists of an integrating sphere of 100 mm in diameter into which a laser is injected by means of an optical fibre. The power of the laser is 20 mW and it is set to a stable reference by the means of a feedback loop. The system is mounted on different translation and rotation stages to allow its full characterisation.

The radiance comparator slit scattering function is first measured by scanning the wavelength of the radiance source over the full spectral bandwidth of the instrument. The comparator is then translated in front of the fixed-point blackbody at the freezing plateau to measure its absolute radiance. The thermodynamic temperature of the fixed point is calculated from the following equation, deduced from the ratio of Planck's Law for the two measurements:

$$T \cong \frac{1}{n_{\text{air}} \cdot \lambda_{\text{eff}}} \frac{c_2}{\ln \left( 1 + \frac{c_1 \cdot S_{\text{laser}} \cdot G_{\text{bb}}}{n_{\text{air}}^2 \cdot \lambda_{\text{eff}}^5 \cdot S_{\text{bb}}(\lambda_{\text{eff}}, T) \cdot G_{\text{laser}} \cdot L_{\text{laser}}(\lambda)} \right)} \quad (2)$$

where:

$c_1$  is the first radiation constant for spectral radiance,  $c_2$  is the second radiation constant,  $n_{\text{air}}$  is the refractive index of air,  $\lambda_{\text{eff}}$  is the effective wavelength of the slit scattering function,  $S_{\text{laser}}$  is the monochromatic source signal as measured by the radiance comparator at the effective wavelength,  $G_{\text{bb}}$  is the radiance comparator amplifier transimpedance,  $S_{\text{bb}}(\lambda_{\text{eff}}, T)$  is the fixed point signal as measured by the radiance comparator at the effective wavelength,  $G_{\text{laser}}$  is the trap detector amplifier transimpedance and  $L_{\text{laser}}(\lambda)$  is the radiance of the monochromatic source.

The comparison between the absolute radiance source and the blackbody is performed by fixing the effective wavelength of the radiance comparator at the wavelength of the laser. The ratio of the two signals is corrected using the optical responsivity of the radiance comparator. This correction is estimated by scanning the spectral bandwidth of the instrument with the monochromator, the comparator being in front of a blackbody.

The absolute radiance of the monochromatic source  $L_{\text{laser}}(\lambda)$ , defined in the equation above, is measured by a so-called “radiancemeter”. The instrument is composed of a trap detector directly calibrated against the cryogenic radiometer, and two precise apertures of 6 mm and 8 mm nominal diameter separated by a known distance. The aperture diameters are measured with a non-contact method, while the distance between them, typically 500 mm, is measured by a precise gauge. The 6-mm aperture is positioned in front of the trap detector. This aperture size was chosen to fit with the photodiode of 10 mm in diameter in order to collect all the radiant flux going through the geometrical extent. A baffle is set up between the sphere source and the trap detector to reduce the stray light detected by the trap detector. The horizontal rotation of the sphere by 90° allows it to be moved so that it can be viewed by both the radiance comparator and the trap detector alternately over a short time period.

Figure 10 shows a 3D drawing of the radiancemeter and the monochromatic source. Both the radiancemeter and the monochromatic source are placed inside a black-painted box to protect them from stray light.

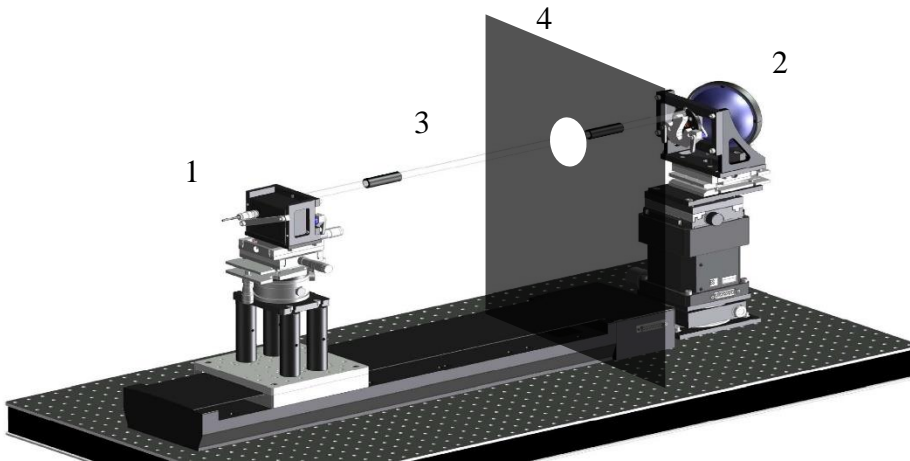


**Figure 10: Radiancemeter and monochromatic source of radiance. Trap detector (1), monochromatic source (2), precise gauge (3), baffle (4)**

This radiance method requires an extensive characterisation of the possible biases and associated uncertainties induced by the radiancemeter such as the radiance stability of the sphere, its spatial homogeneity, and the stray light detected by the trap; as well as those associated with the radiance comparator such as the linearity, size-of-source effect and the out-of-band transmittance.

### 3.2.4.2 Target uncertainty budgets for the LNE-Cnam measurements

Table 10 shows the uncertainty components  $u(T_{Zn})$ ,  $u(T_{Al})$  and  $u(T_{Ag})$  at the fixed points of zinc, aluminium and silver respectively and the combined uncertainty. The intermediate quadratic sums of the main components that relate to each instrument (radiancemeter, radiance comparator and fixed points) are shown.

**Table 10: Uncertainty budget  $u(T_{Zn})$ ,  $u(T_{Al})$  and  $u(T_{Ag})$  for the thermodynamic temperatures  $T_{Zn}$ ,  $T_{Al}$  and  $T_{Ag}$  measured at LNE-Cnam at 1550 nm using an InGaAs trap detector as the radiometric reference**

Component	Uncertainty	Unit	$u(T_{Zn})$ /mK	$u(T_{Al})$ /mK	$u(T_{Ag})$ /mK
$\lambda_{laser}$ (air)	$5.0 \times 10^{-12}$	m	0	0	1
Trap response	$3.3 \times 10^{-5}$	V	10	19	33
Amplifier ( $G_{laser}$ )	$1.0 \times 10^2$	$\Omega$	1	9	16
Trap responsivity	$6.0 \times 10^{-4}$	A/W/m	31	56	99
Distance between apertures	$3.5 \times 10^{-6}$	m	0	1	2
$r_1$ (radius aperture sphere)	$2.5 \times 10^{-7}$	m	5	8	15
$r_2$ (radius aperture trap)	$2.5 \times 10^{-7}$	m	6	11	19
$K$ diffusion (stray light)	$6.0 \times 10^{-4}$	1	20	38	66
$K$ sphere inhomogeneity	$1.0 \times 10^{-4}$	1	5	9	16
<b>Total (radiancemeter) (<math>k = 1</math>)</b>			<b>39</b>	<b>73</b>	<b>128</b>
Effective wavelength $\lambda_{eff}$	$5.0 \times 10^{-12}$	m	2	3	4
Slit scattering function ( $\lambda_{eff}$ )	$4.6 \times 10^{-13}$	V.m	10	19	33
Amplifier (sphere) ( $G_{BB}$ )	$1.0 \times 10^3$	$\Omega$	5	9	16
Response comparator $S_{bb}$	$1.4 \times 10^{-5}$	V	4	4	11
Amplifier (FP) ( $G_{BB}$ )	$9.9 \times 10^3$	$\Omega$	5	9	16
$K_{OOB}$	$6.0 \times 10^{-5}$	1	3	6	10
$K_{SSE}$	$2.0 \times 10^{-5}$	1	1	2	3
<b>Total radiance comparator (<math>k = 1</math>)</b>			<b>14</b>	<b>24</b>	<b>43</b>
Emissivity	$1 \times 10^{-4}$	1	2	3	5
Impurities	$5 \times 10^{-6}$	1	5	5	5
Setpoint / plateau repeatability		1	5	8	10
<b>Total fixed point (<math>k = 1</math>)</b>		1	<b>7</b>	<b>10</b>	<b>12</b>
Day to day repeatability		1	5	22	17
<b>Combined uncertainty (<math>k=1</math>)/ mK</b>			<b>42</b>	<b>77</b>	<b>136</b>
<b>Expanded uncertainty (<math>k = 2</math>)/ mK</b>			<b>84</b>	<b>154</b>	<b>272</b>

The uncertainty components relating to the radiancemeter are defined as follows:

- $\lambda_{\text{laser}}$  refers to the uncertainty associated with the wavelength laser stability
- *Trap response* refers to the stability of the trap within a daily measurement
- *Amplifier* refers to the amplifier transimpedance uncertainty for the trap detector
- *Trap responsivity* refers to the uncertainty of the calibration of the trap detector, including the spatial homogeneity, the stability during the calibration process and the repeatability of the measurements
- *Distance between apertures* is the uncertainty associated to the distance that separates the two apertures
- $r_1$  and  $r_2$  are the uncertainty components associated to the radius of the sphere and the trap apertures respectively
- *K diffusion* is the uncertainty associated to the correction of the stray light in the radiancemeter
- *K sphere inhomogeneity* is the uncertainty associated to the correction of the radiance inhomogeneity in the plane of the sphere aperture

The uncertainty components relating to the radiance comparator are defined as follow:

- *Effective wavelength* refers to the uncertainty associated to the wavelength stability of the laser
- *Slit scattering function* is the uncertainty that refers to the repeatability of the slit scattering function integral, defined by  $\int_{\lambda_{p1}}^{\lambda_{p2}} L_{\text{laser}}(\lambda_{\text{laser}} - \lambda_p) d\lambda_p$  where  $L_{\text{laser}}(\lambda_{\text{laser}} - \lambda_p)$  is the spectral radiance of the sphere measured by the radiance comparator at the effective wavelength  $\lambda_p$ .  $[\lambda_{p2} - \lambda_{p1}]$  is the spectral range of integration defined by the interference filter used to cut the out-of-band transmittance of the monochromator
- *Amplifier (sphere)* refers to the uncertainty of the amplifier of the radiance comparator when it measures the sphere radiance
- *Response comparator* is the uncertainty component related to the stability of the radiance comparator response, when a fixed point is measured at the effective wavelength  $\lambda_p = \lambda_{\text{laser}}$
- *Amplifier (FP)* refers to uncertainty of the amplifier of the radiance comparator when it measures the fixed point
- $K_{\text{OBB}}$  is the uncertainty associated to the correction of the out of band transmittance of the monochromator
- $K_{\text{SSE}}$  is the uncertainty associated to the correction of the size-of-source-effect of the radiance comparator

The uncertainty components relating to the fixed points are defined as follow:

- *Emissivity* is the uncertainty in determining the total emissivity of the cavity
- *Impurities* is the uncertainty due to the ingot impurities in the 5N pure metal as claimed by the supplier
- *Set point / plateau repeatability* is the uncertainty due to the reproducibility of the freezing plateaux including the change of the furnace set points to initiate the phase change
- *Day to day repeatability* is the standard deviation of repeated measurements

### 3.2.5 Measurements at PTB

#### 3.2.5.1 Equipment and methodology

Measurements at PTB are being performed using a four-wavelength ratio filter radiometer (FRFR), which operates at four distinct wavelengths between 440 nm and 1550 nm (Table 11) and is comprised of three silicon photodiodes and one InGaAs photodiode. The arrangement consists of four separate filter radiometers mounted on a linear stage with a common 3 mm diameter aperture, as shown in Figure 11 [28].

**Table 11: Characteristics of the four FRs used within the FRFR**

Centre wavelength	440 nm	650 nm	900 nm	1550 nm
Photodiode	Si	Si	Si	InGaAs

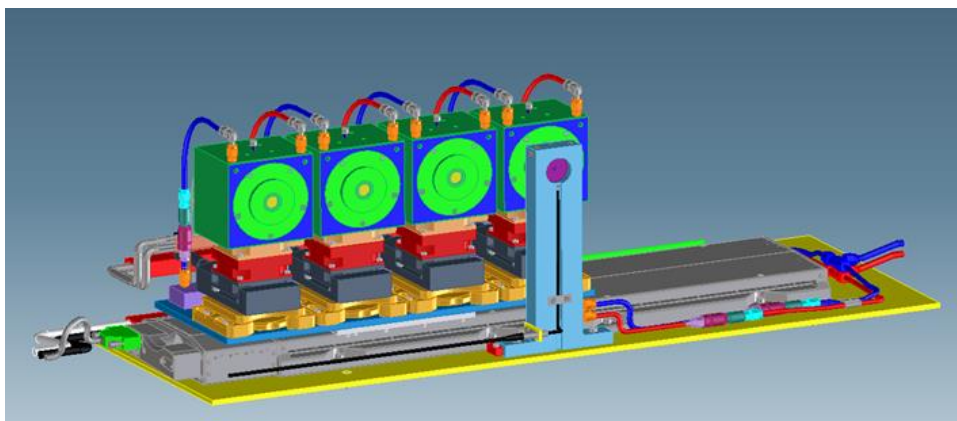


**Figure 11: A schematic of the four-wavelength filter radiometer system**

For a simplified calibration an additional reference detector can be set up on the radiometers' linear stage. The calibration of the filter radiometer itself is a two-step process. First, a broadband transfer detector (Si trap detector or InGaAs single photodiode) is calibrated against a cryogenic radiometer at several discrete laser emission lines. Then the transfer detector is used to continuously calibrate the filter radiometers at a spectral comparator. The main principles of the calibration process are described in detail in [29]. The resulting spectral responsivity of each of the four filter radiometers is presented in Figure 12.

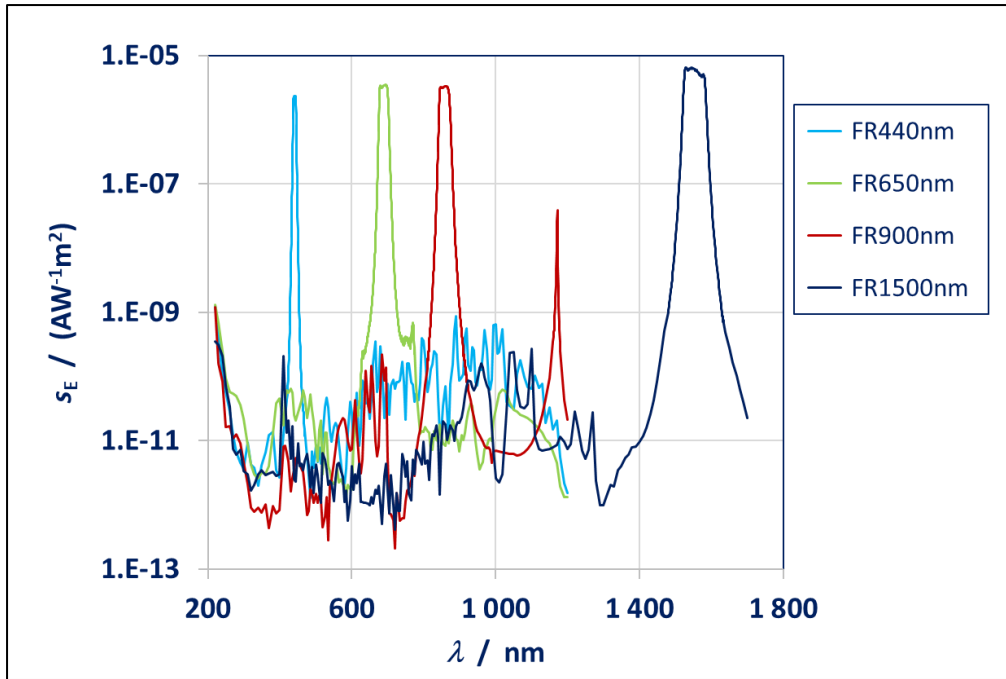


Figure 12: Schematic of the operational wavelength bands of the filter radiometer system

For thermodynamic temperature measurements, the filter radiometers will be set up with PTB's large area blackbody (LABB). This blackbody furnace has been developed for accurate realisation of the spectral irradiance in the red and near-infrared spectral ranges. Its temperature is measured by standard platinum resistance thermometers according to the International Temperature Scale of 1990 (ITS-90). The blackbody consists of two concentric sodium heat pipes, the inner one with temperature stability of a few millikelvin forming the radiating cavity. The filter radiometer will also be used to measure  $T - T_{90}$  using the double heat pipe blackbody source (Figure 13 and [30, 31]).

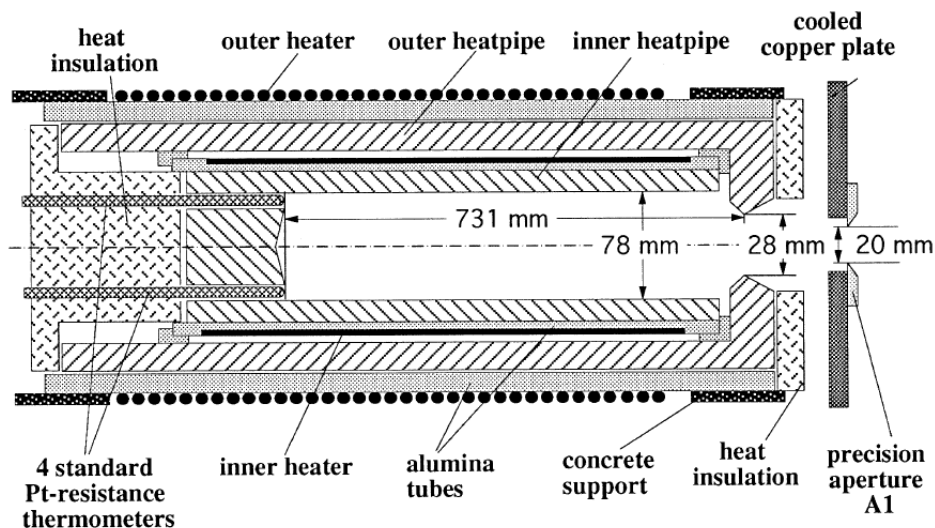


Figure 13: Schematic drawing (not to scale) of the double-heat pipe blackbody [from 30, 31]

### 3.2.5.2 Target uncertainties

An overview of the measurement uncertainties with respect to ITS-90 temperature determination of the LABB using the SPRTs is given in the Table below. The expected combined measurement uncertainty for  $T_{90}$  varies between 24 mK and 62 mK between 692 K and 1235 K ( $k = 2$ ).

**Table 12: Expected uncertainty budget for the determination of the ITS-90 temperature of the large area blackbody (LABB)**

<b>Uncertainty contribution (<math>k = 1</math>)</b>	<b>At Zn point <math>u</math>/ mK</b>	<b>At Al point <math>u</math>/ mK</b>	<b>At Ag point <math>u</math> / mK</b>
Realisation of $t_{90}$	3	5	10
Gradient at cavity bottom	2	3	5
Stability of LABB	10	4	25
Stability of SPRT	5	10	15
Self heating of SPRT	2	2	2
<b>Combined (<math>k = 1</math>)/ mK</b>	<b>12</b>	<b>12</b>	<b>31</b>
<b>Expanded (<math>k = 2</math>)/ mK</b>	<b>24</b>	<b>24</b>	<b>62</b>

For the spectral irradiance measurement the expected relative uncertainty components are given in Table 13. The uncertainties originate from the measurement geometry (distance measurement, aperture area, diffraction correction), the filter radiometer calibration (which varies spectrally as the uncertainty of the reference detectors increases considerably towards the near infrared), and the measurement in front of the LABB (random uncertainty, emissivity, repeatability, amplifier gain).

For temperatures of 692 K, 933 K and 1235 K the corresponding temperature uncertainty is calculated for two filter radiometers with a centre wavelength at 900 nm and 1550 nm respectively. For the filter radiometer at 1550 nm the uncertainties range between 440 mK at 1235 K and 138 mK at 692 K ( $k = 2$ ). For the 900 nm filter radiometer the expected measurement uncertainties are 120 mK at 1235 K and 68 mK at 933 K ( $k = 2$ ). At 692 K a relatively high signal-to-noise ratio is expected for the 900 nm filter radiometer and this temperature point will be omitted for this filter radiometer.

The differences in achievable measurement uncertainty illustrate well-known principles in radiation thermometry (which can be derived from Planck's law of thermal radiation): the centre wavelength of the filter radiometer should be chosen to be as short as possible in order to achieve a low temperature uncertainty from a given uncertainty in spectral irradiance. Yet, the spectral irradiance of a blackbody decreases with decreasing wavelength on the short wavelength side of its maximum and consequently, the uncertainty of the radiance below a certain radiance level is dominated by the limited detectivity of the detector in the filter radiometer.

**Table 13: Uncertainty budget for the spectral irradiance measurements**

Source of uncertainty	FR 900	FR 1550
	/ 10 <sup>-4</sup>	/ 10 <sup>-4</sup>
<b>Type A: Random</b>		
Random uncertainty	2	2
<b>Type B: Systematic</b>		
Diffraction of trap and FR	1	1
Distance measurement	1	1
Amplifier gain	2	2
Repeatability	1	1
Aperture area	2	2
Emissivity LABB	2	2
FR Calibration	4	13
Diffraction BB aperture	2	2
<b>Sum in quadrature, relative standard uncertainty</b>	<b>6</b>	<b>14</b>
Temperature equivalent at Zn point/ mK ( $k = 1$ )	-	69
Temperature equivalent at Al point/ mK ( $k = 1$ )	34	126
Temperature equivalent at Ag point/ mK ( $k = 1$ )	60	220
<b>Temperature equivalent at Zn point/ mK (<math>k = 2</math>)</b>	<b>-</b>	<b>138</b>
<b>Temperature equivalent at Al point/ mK (<math>k = 2</math>)</b>	<b>68</b>	<b>252</b>
<b>Temperature equivalent at Ag point/ mK <math>k = 2</math></b>	<b>120</b>	<b>440</b>

Another measurement principle in radiation thermometry allows the determination of the temperature of a blackbody at unknown temperature  $T_x$  using a blackbody of known temperature  $T_{ref}$  by a ratio measurement of spectral radiance using Planck's law of thermal radiation. The measurement uncertainty then propagates according to:

$$U(T_x) = \left(\frac{T_x}{T_{ref}}\right)^2 U(T_{ref}) \quad (3)$$

Thus, the uncertainty  $U(T_x)$  is larger than  $U(T_{ref})$  for  $T_x > T_{ref}$ , and smaller than  $U(T_{ref})$  for  $T_x < T_{ref}$ . Consequently, the low measurement uncertainty at 1235 K with the FR900 can be utilised towards lower temperatures by using the FR1550 for a spectral irradiance ratio measurement of the LABB operated at 692 K and 933 K with respect to 1235 K (the reference temperature measured with FR900).

The resulting expected measurement uncertainties for  $T$  at 692 K and 933 K are given in Table 14.

**Table 14: Expanded uncertainty estimates of the LABB at lower temperatures by extrapolating down in temperature from the silver point (1235 K) at 900 nm**

	$U (k = 2)/ \text{mK}$
At Ag point (FR 900 and FR 1550)	<b>120</b>
At Al point (FR 1550)	<b>68</b>
At Zn point (FR 1550)	<b>38</b>

### 3.2.6 Measurements at NIM

For measuring the spectral radiance of the Ag fixed point directly, a new design of absolute radiation thermometer (ART) was established at NIM. This system consists of a 50 mm diameter chromatic doublet lens with 400 mm focal length, a 20 mm diameter knife-edge aperture behind the lens and a filter radiometer at a distance of 1400 mm from the lens. In the ART, the 900 nm filter radiometer (called FR900 in the text), which has a peak wavelength of 900 nm and a bandwidth of 40 nm, was used to determine the temperature of the Ag fixed point blackbody. The arrangement is shown schematically in Figure 14.

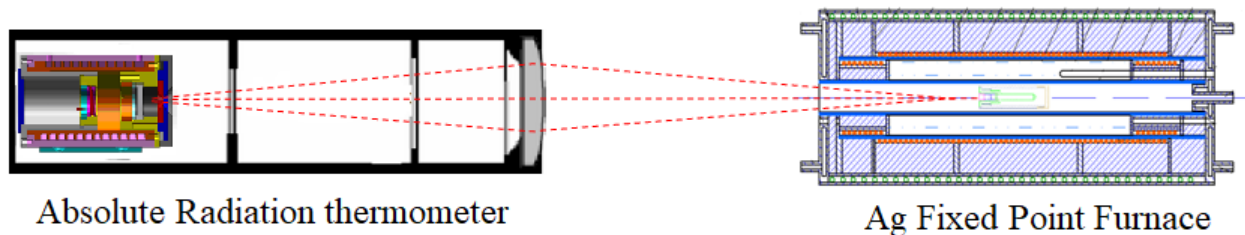


Figure 14: A schematic of the absolute radiation thermometer and the Ag fixed point furnace

The irradiance responsivity of the FR900 was calibrated at PTB and NIM. The results were compared and are shown in Figure 15.

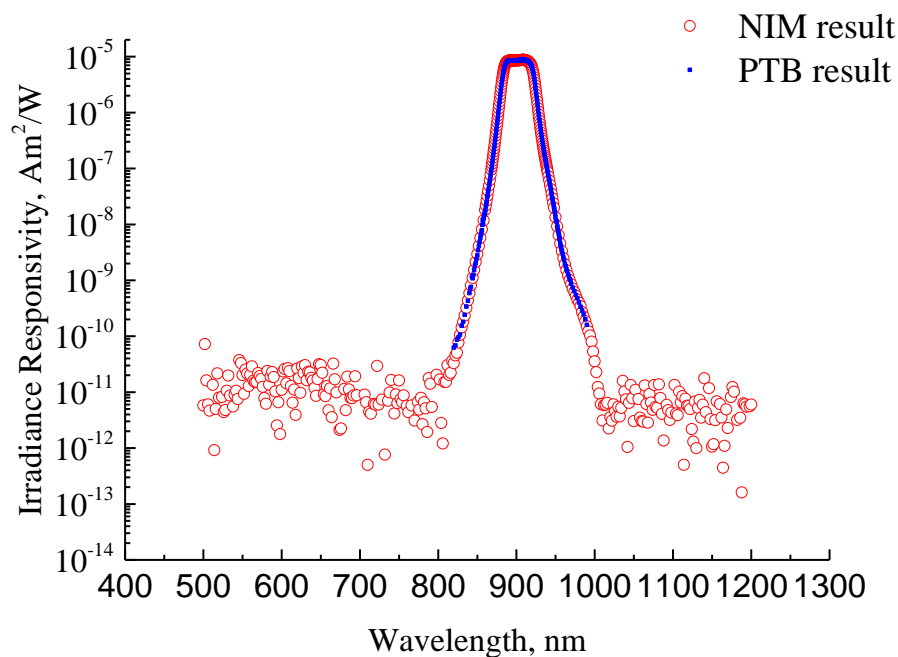


Figure 15: Irradiance responsivity of the filter radiometer FR900

The uncertainty components associated with the FR900 are given in Table 15, and the corresponding uncertainties associated with the measurements of the Ag fixed point, expressed in terms of kelvin, are given in Table 16.

**Table 15: Relative uncertainty associated with the absolute radiation thermometer (ART) when measuring fixed-point cells**

Source of uncertainty	FR900
Integral of FR	$8.4 \times 10^{-4}$
Correction of non-linearity	$5.0 \times 10^{-4}$
Lens transmittance	$2.4 \times 10^{-4}$
Effective area of the blackbody	$3.0 \times 10^{-4}$
Lens aperture area	$1.4 \times 10^{-4}$
Distance of aperture	$1.0 \times 10^{-4}$
Digital voltmeter and amplifier	$1.0 \times 10^{-4}$
Air index	$0.2 \times 10^{-4}$
<b>Combined standard uncertainty (<math>k = 1</math>)</b>	<b><math>1.1 \times 10^{-3}</math></b>

**Table 16: Uncertainties of the freezing point of Ag**

Source of uncertainty	At Ag/ mK
Calibration of ART	120
Wavelength/ 0.02nm	10
FP realisation	10
Repeatability	40
<b>Combined standard uncertainty (<math>k = 1</math>)/ mK</b>	<b>130</b>
<b>Total expanded uncertainty (<math>k = 2</math>)/ mK</b>	<b>260</b>

The silver fixed point was measured by the ART following its calibration and characterisation. A dual direction laser was used to help the alignment of the ART with the furnace. The image of the cell aperture was observed directly on the cover of the filter radiometer aperture. The measurement results of the fixed point and uncertainties are shown in Table 17 below.

**Table 17: Results and uncertainty for  $T$  measurements at the Ag fixed-point**

Fixed point	$T/ K$	$U (k = 2)/ mK$
Ag	1234.84	260

## 4 CONCLUSIONS

Under the auspices of the EMPIR InK2 project measurements of  $T - T_{90}$  are being carried by a number of different NMIs over the temperature range from 430 K to 1358 K using two thermodynamic techniques: acoustic gas thermometry and primary radiation thermometry or radiometry, as summarised below (note that all uncertainties are expressed as  $k = 2$ ).

Acoustic gas thermometry measurements are being carried out at NPL using an aluminium cylindrical resonator to higher temperatures than the measurements carried out in the InK1 project. Measurements of  $T - T_{90}$  using relative primary acoustic gas thermometry are anticipated to produce thermodynamic temperature estimates with uncertainties of just a few mK. An additional resonator has been constructed out of CuCrZr has greater hardness than copper and will enable the measurement range to be extended further, up to 873 K.

At NIM a cylindrical acoustic resonator is being used with the aim of extending acoustic gas thermometry up to 1358 K. Heat pipes are being used to provide a uniform and stable environment for the cylindrical cavity. Target measurement uncertainties at 500 K, 1000 K and 1358 K are 10 mK, 50 mK and 120 mK, respectively ( $k = 2$ ).

In addition,  $T - T_{90}$  measurements are being performed at NPL using primary radiation thermometry, using an InGaAs-based radiation thermometer operating at around 1600 nm, a set of fixed-point cells, a bespoke pressure-controlled heat pipe system and a passive caesium heat pipe. Together these can cover the temperature range from 505 K to 1358 K. The thermodynamic temperature,  $T$ , of the sources is determined from the spectral response of the radiation thermometer anchored to a gold fixed-point blackbody with an assigned  $T = 1337.36$  K (as measured at NIST). The target expanded uncertainties were estimated and range from around 30 mK for measurements with the lower temperature fixed points (Sn, Zn) up to around 200 mK for measurements with the Na PCHP at the Ag point.

$T - T_{90}$  measurements are being performed at CEM using two absolutely calibrated standard radiation thermometers, namely an LP4 operating at 650 nm and 900 nm and an LP5 operating at 1550 nm, along with Cu, Ag and Zn fixed points and VTBBs. The calibration of the standard thermometers is via a Si trap radiometer and an InGaAs radiometer which are calibrated absolutely at IO-CSIC with an electrical substitution cryogenic radiometer.  $T$  may be determined either by absolute primary radiation thermometry or relative primary radiation thermometry using a silver fixed-point blackbody with assigned  $T = 1234.90$  K. All the uncertainties have been calculated for both methods and thermometers. The best expanded uncertainties range from 80 mK to 190 mK, from 673 K to 1358 K. The relative primary thermometry gives better uncertainties than absolute primary thermometry at  $T < 1223$  K, due to the large calibration uncertainty at 900 nm and 1550 nm – where  $U$  (absolute responsivity of the standard radiometers) is 0.15%, twice the uncertainty at 650 nm (0.075%).

$T - T_{90}$  measurements are being performed at LNE-Cnam using a monochromator-based radiance comparator which has been adapted to the infrared spectral range (1600 nm). Measurements of  $T$  of the blackbody source (FPB or VTBB) is performed by comparing the radiance of the source with that of an integrating sphere, whose radiance is measured, in turn, with a transfer trap detector calibrated using the LNE-Cnam cryogenic radiometer. Target expanded uncertainties for the  $T - T_{90}$  measurements range from 84 mK with the Zn fixed point (692 K) to 272 mK with the Ag fixed point (1235 K).

$T - T_{90}$  measurements are being carried out at PTB using a four-wavelength radiometer which operates at four distinct wavelengths between 440 nm to 1550 nm. The radiometers are calibrated with reference to a transfer detector which has been calibrated against a cryogenic radiometer.  $T - T_{90}$  measurements are being carried out using a large area double heat pipe VTBB. For absolute primary radiation thermometry, target uncertainties are from around 440 mK at 1235 K to around 140 mK at 692 K for the 1550 nm radiometer, and from around 70 mK at 933 K to 120 mK at 1235 K for the 900 nm radiometer. Relative primary radiation thermometry towards lower temperatures can be carried out with the 1550 filter radiometer, by using reference measurements at around 1235 K with the 900 nm filter radiometer. The resultant target expanded uncertainties range between 38 mK at 692 K to 120 mK at 1235 K.

Measurements at NIM are being carried out using an absolute radiation thermometer operating at 900 nm. This is being used to measure the thermodynamic temperature of a silver fixed-

point blackbody ( $T_{90} = 1234.93$  K). The target uncertainty for the measurements of the silver cell is 260 mK ( $k = 2$ ).

Once all the measurements have been completed the results will be pooled in order to provide provisional estimated values of  $T - T_{90}$  over the whole range from 430 K to 1358 K for submission to the Consultative Committee on Thermometry (CCT). By pooling all the data it is hoped that it will be possible to achieve lower uncertainties than are achievable by one laboratory operating in isolation.

## 5 ACKNOWLEDGEMENTS

This work has received funding from the EMPIR programme co-financed by the Participating States and from the European Union's Horizon 2020 R&I programme through the InK2 project.

NIM's research was supported by the National Key R&D Program of China (number 2016YFF0200101)

## 6 REFERENCES

[1] <https://www.bipm.org/en/committees/cc/cct/guide-its90.html>

[2] Fischer J, de Podesta M, Hill K D, Moldover M, Pitre L, Rusby R, Steur P, Tamura O, White R and Wolber L 2011 Present Estimates of the Differences Between Thermodynamic Temperatures and the ITS-90 *Int. J. Thermophys.* **32** 12-25

[3] Machin G, Engert J, Gavioso R, Sadli M and Woolliams E 2016 Summary of achievements of the EMRP project implementing the new kelvin (InK) *Measurement* **94** 149-156

[4] Woolliams E R et al 2016 Thermodynamic temperature assignment to the point of inflection of the melting curve of high-temperature fixed points *Phil. Trans. R. Soc. A* **374**: 20150044

[5] Moldover M R, Gavioso R M, Mehl J B, Pitre L, de Podesta M and Zhang J T 2014 Review article - Acoustic gas thermometry *Metrologia* **51** R1–R19

[6] Underwood R, de Podesta M, Sutton G, Stanger L, Rusby R, Harris P, Morantz P and Machin G 2017 Further estimates of  $(T - T_{90})$  close to the triple point of water *Int J Thermophys* **38** 44

[7] Underwood R, Sutton G, de Podesta M, Stanger L, Rusby R, Harris P, Morantz P and Machin G 2016 Estimates of the difference between thermodynamic temperature and the ITS-90 in the range 118 K to 303 K *Phil. Trans. R. Soc. A* **374**: 20150048

[8] Underwood R J and Edwards G J 2014 Microwave-dimensional measurements of cylindrical resonators for primary acoustic thermometry *Int. J. Thermophys.* **35** 971

[9] Feng X J, Gillis KA, Moldover M R and Mehl J B 2013 Microwave-cavity measurements for gas thermometry up to the copper point *Metrologia* **50** 219–226

- [10] Zhang K, Feng X J, Gillis K A et al 2016 Acoustic and microwave tests in a cylindrical cavity for acoustic gas thermometry at high temperature *Phil. Trans. R. Soc. A* **374**: 20150049
- [11] Zhang K, Feng X J et al 2017 Microwave measurements of the length and thermal expansion of a cylindrical resonator for primary acoustic gas thermometry *Meas Sci Technol* **28**: 015006
- [12] Chen H H, Feng X J, et al 2019 Optimization of acoustic waveguides for acoustic gas thermometry *Acta Metrologica Sinica* **40** 1-7 (in Chinese) doi:10.3969/j.issn.1000-1158.2019.01.01
- [13] Gillis K, Lin H and Moldover M 2009 Perturbations from ducts on the modes of acoustic thermometers *J Res Natl Inst Stand Technol* **114** 263-285
- [14] Zheng R W 2016 Investigation on precision measurement of thermal expansion coefficient for cavity based on microwave resonance. Thesis for Master degree. Changchun University of Science and Technology. (in Chinese)
- [15] Anhalt K and Machin G 2016 Thermodynamic temperature by primary radiometry *Phil. Trans.R. Soc. A* **374**, 20150041
- [16] Hartmann J 2009 High-temperature measurement techniques for the application in photometry, radiometry and thermometry *Phys. Rep.* **469** 205-269
- [17] Machin G, Bloembergen P, Anhalt K, Hartmann J, Sadli M, Saunders P, Woolliams E, Yamada Y and Yoon H 2010 Practical implementation of the mise en pratique for the definition of the kelvin above the silver point *Int. J. Thermophys.* **31**, 1779-1788
- [18] Yoon H W, Gibson C E, Khromchenko V and Eppeldauer G P 2007 SSE- and noise-optimized InGaAs radiation thermometer *Int. J. Thermophys.* **28** 2076-2086
- [19] Brown S W, Eppeldauer G P and Lykke K R 2006 Facility for spectral irradiance and radiance responsivity calibrations using uniform sources *Applied Optics* **45** 8218-8237
- [20] McEvoy H C, Sadli M, Bourson F, Briaudeau S and Rougié B 2013 A comparison of the NPL and LNE-Cnam silver and copper fixed-point blackbody sources, and measurement of the silver/copper temperature interval *Metrologia* **50** 559-571
- [21] Saunders P, Fischer J, Sadli M et al 2008 Uncertainty budgets for calibration of radiation thermometers below the silver point *Int J Thermophys* **29** 1066-1083
- [22] Fischer J, Neuer G, Schreiber E and Thomas R 2002 Metrological characterisation of a new transfer-standard radiation thermometer *Proceedings of the 8th International Symposium on Temperature and Thermal Measurements in Industry and Science (Berlin, Germany)* (Berlin: VDE VERLAG GmbH) 801-806
- [23] Schreiber E and Neuer G 2005 Reduction of the size-of-source effect and distance dependency of a high precision infrared radiation thermometer *Proceedings of the 9th International Symposium on Temperature and Thermal Measurements in Industry and Science (Cavtat – Dubrovnik, Croatia)* (Zagreb: LPM/ FSB) 527-532

- [24] Martin M J, Mantilla J M, del Campo D, Herranz M L, Pons A and Campos J 2017 Performance of different light sources for the absolute calibration of radiation thermometers *Int J Thermophys* **38**, 138
- [25] Bloembergen P, Duan Y, Bosma R and Yuan Z 1997 The characterization of radiation thermometers subject to the size-of-source effect *Proceedings of the 6<sup>th</sup> International Symposium on Temperature and Thermal Measurements in Industry and Science (Turin, Italy)* (Torino: Levrotto & Bella) 261-266
- [26] Saunders P, Woolliams E, Yoon H, Todd A, Sadli M, van der Ham E, Anhalt K, Werner L, Taubert D R, Briaudeau S and Khlevnoy B May 2018 Uncertainty estimation in primary radiometric temperature measurement *CC-WG-NCTh document*
- [27] Machin G, Anhalt K, Bloembergen B, Hartmann J, Sadli M, Saunders P, Woolliams E, Yamada Y and Yoon H (Document CCT/10-12)  
[http://www.bipm.org/cc/CCT/Allowed/25/MeP\\_HT\\_v9.1.doc](http://www.bipm.org/cc/CCT/Allowed/25/MeP_HT_v9.1.doc) (Accessed 6 March 2014)
- [28] Wähler M et al. 2017 Thermodynamic temperature of high-temperature fixed points traceable to blackbody radiation and synchrotron radiation *Int J Thermophys* **38**: 144
- [29] Taubert, D R, Friedrich R, Hartmann J, and Hollandt J. 2003 Improved calibration of the spectral responsivity of interference filter radiometers in the visible and near infrared spectral range at PTB *Metrologia* **40** S35-S38
- [30] Fischer J, Seidel J and Wende B 1998 The double-heatpipe black body: a radiance and irradiance standard for accurate infrared calibrations in remote sensing *Metrologia* **35** 441-446
- [31] Stock M, Fischer J, Friedrich R, Jung H J and Wende B 1995 The double-heatpipe black body: a high-accuracy standard source of spectral irradiance for measurements of  $T - T_{90}$  *Metrologia* **32** 441-444